nature medicine

A microRNA screen reveals that elevated hepatic ectodysplasin A expression contributes to obesity-induced insulin resistance in skeletal muscle

Motoharu Awazawa[1–3], Paula Gabel[1–3], Eva Tsaousidou[1–3], Hendrik Nolte[3], Marcus Krüger[3], Joel Schmitz[1–3], P Justus Ackermann[1–3], Claus Brandt[1–3], Janine Altmüller[4,5], Susanne Motameny[4], F Thomas Wunderlich[1], Jan-Wilhelm Kornfeld[1,3], Matthias Blüher[6] & Jens C Brüning[1–3,7]

Over 40% of microRNAs (miRNAs) are located in introns of protein-coding genes, and many of these intronic miRNAs are co-regulated with their host genes[1,2]. In such cases of co-regulation, the products of host genes and their intronic miRNAs can cooperate to coordinately regulate biologically important pathways[3,4]. Therefore, we screened intronic miRNAs dysregulated in the livers of mouse models of obesity to identify previously uncharacterized protein-coding host genes that may contribute to the pathogenesis of obesity-associated insulin resistance and type 2 diabetes mellitus. Our approach revealed that expression of both the gene encoding ectodysplasin A (*Eda*), the causal gene in X-linked hypohidrotic ectodermal dysplasia (XLHED)[5], and its intronic miRNA, miR-676, was increased in the livers of obese mice. Moreover, hepatic *EDA* expression is increased in obese human subjects and reduced upon weight loss, and its hepatic expression correlates with systemic insulin resistance. We also found that reducing miR-676 expression in *db*/*db* mice increases the expression of proteins involved in fatty acid oxidation and reduces the expression of inflammatory signaling components in the liver. Further, we found that *Eda* expression in mouse liver is controlled via PPARγ and RXR-α, increases in circulation under conditions of obesity, and promotes JNK activation and inhibitory serine phosphorylation of IRS1 in skeletal muscle. In accordance with these findings, gain- and loss-of-function approaches reveal that liver-derived EDA regulates systemic glucose metabolism, suggesting that EDA is a hepatokine that can contribute to impaired skeletal muscle insulin sensitivity in obesity.

In order to explore the potential role of host genes in liver that are co-regulated with intragenic miRNAs showing altered expression in obesity, we first reanalyzed previously reported microarray expression data for hepatic miRNAs in obese mice[6]. Of 70 miRNAs upregulated in the livers of both *db*/*db* mice and high-fat diet (HFD)-fed obese mice as compared to their lean controls (**Supplementary Table 1**), 34 were identified as intragenic (**Supplementary Table 2**). Of these, we selected for further analysis six obesity-regulated intragenic miRNAs whose host genes had not been previously investigated in the context of metabolic regulation (**Supplementary Table 3**). In comparisons of the host protein-coding genes to these six miRNAs (**Fig. 1a**), only *Eda*, corresponding to *Mir676*, exhibited greater expression in the livers of an independent cohort of *db*/*db* mice as compared to corresponding lean *misty*/*misty* controls (Online Methods and **Fig. 1b**). We observed relatively ubiquitous expression of *Eda* mRNA and miR-676-3p, the dominant miRNA originating from the *Mir676* locus, in wild-type mouse tissues (**Supplementary Fig. 1a**). However, the obesity-associated increase in expression of these RNAs occurred exclusively in the liver in both *db*/*db* mice and mice with HFD-induced obesity as compared to their respective lean controls (**Fig. 1c–f**). In the livers of the obese mouse models, upregulation of EDA protein was further confirmed by immunoblotting (**Fig. 1g**), as was miR-676 upregulation by northern blotting and miRNA-seq (**Supplementary Fig. 1b,c**). Analyses of fractionated parenchymal and nonparenchymal liver cells from *db*/*db* mice showed greater expression of *Eda* and miR-676 as compared to that of lean *misty*/*misty* controls only in the hepatocyte fraction, but not in the nonparenchymal cell fraction (**Supplementary Fig. 2a**).

EDA belongs to a family of cytokines related to tumor necrosis factor (TNF)[7] and is cleaved by furin, a ubiquitously expressed endoprotease, before extracellular secretion[8]. Given that TNF concentrations increase in the circulation of obese mice[9], we next investigated whether EDA could also act as a hepatokine whose concentration might be higher in the circulation of obese mice. Overexpression of human EDA-A1 (hEDA) in mouse Hepa 1-6 hepatoma cells led to release of cleaved EDA protein into the supernatant, which was abrogated in cells expressing EDA protein in which the furin-recognition site

[1]Department of Neuronal Control of Metabolism, Max Planck Institute for Metabolism Research, Cologne, Germany. [2]Center for Endocrinology, Diabetes and Preventive Medicine (CEDP), University Hospital Cologne, Cologne, Germany. [3]Excellence Cluster on Cellular Stress Responses in Aging-Associated Diseases (CECAD) and Center for Molecular Medicine Cologne (CMMC), University of Cologne, Cologne, Germany. [4]Cologne Center for Genomics (CCG), University of Cologne, Cologne, Germany. [5]Institute of Human Genetics, University Hospital Cologne, Cologne, Germany. [6]Department of Medicine, University of Leipzig, Leipzig, Germany. [7]National Center for Diabetes Research (DZD), Neuherberg, Germany. Correspondence should be addressed to J.C.B. (bruening@sf.mpg.de).

Received 7 July 2016; accepted 11 September 2017; published online 6 November 2017; doi:10.1038/nm.4420

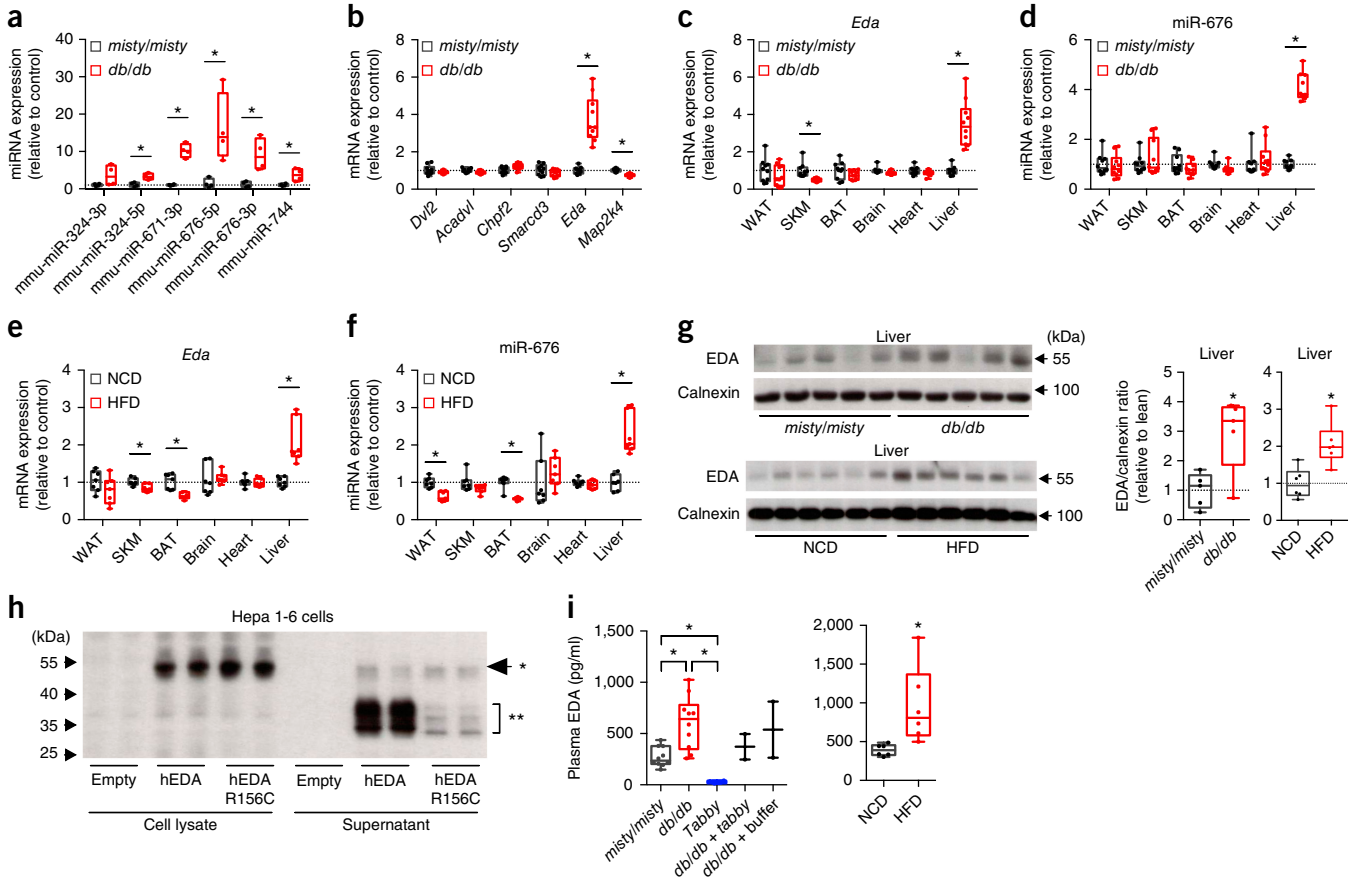

Figure 1 Greater hepatic *Eda* and miR-676 expression in obese mice. (**a**,**b**) Relative expression of intragenic miRNAs determined by miRNA microarray analyses (**a**) and corresponding host protein-coding genes determined by RT–PCR analyses (**b**) in the livers of *db*/*db* mice as compared to lean control mice ($n = 4$ and 10 for each group in **a** and **b**). (**c**,**d**) Expression of *Eda* mRNA (**c**) and miR-676 (**d**) in different tissues of *misty*/*misty* control and *db*/*db* mice as determined by RT–PCR analyses ($n = 10$ for each group). (**e**,**f**) Expression of *Eda* mRNA (**e**) and miR-676 (**f**) in different tissues of normal chow diet (NCD)- and HFD-fed mice as determined by RT–PCR analyses ($n = 7$ for each group). WAT, white adipose tissue; SKM, skeletal muscle; BAT, brown adipose tissue. (**g**) Immunoblots showing EDA and calnexin expression in the livers of *misty*/*misty* control and *db*/*db* mice (upper left) ($n = 5$ for each group) and the livers of NCD- and HFD-fed mice (lower left) ($n = 6$ for each group) together with quantification (right). (**h**) Immunoblot of parental (*; 55-kDa) and cleaved (**; 35-kDa) EDA protein in the cell lysate and supernatant of cultured Hepa 1-6 cells transfected with empty vector or vector encoding full-length hEDA or mutated hEDA (hEDA R156C). The image is representative of three independent experiments. (**i**) Plasma EDA concentrations of *db*/*db* mice as compared to *misty*/*misty* control mice ($n = 10$ for each group) and *Tabby Eda*-deficient mice ($n = 4$) at 8 weeks of age and of HFD-fed as compared to NCD-fed mice at 36 weeks of age ($n = 6$ for each group). Significance was determined by unpaired, two-tailed Student's *t*-test with correction for multiple comparisons via the Holm–Sidak method when applicable in **a**–**g** and by one-way ANOVA with the Holm–Sidak multiple-comparisons test in **i**: $^*P < 0.05$. For box-and-whisker plots: perimeters, 25th–75th percentile; midline, median; whiskers, minimum to maximum values; individual data points are represented. Gene and protein expression are presented as relative values normalized to the mean of the control.

was mutated (hEDA R156C; **Fig. 1h**), indicating that hepatocytes have the ability to secrete EDA. In accordance with these observations, enzyme-linked immunosorbent assay (ELISA)-based assessment revealed greater EDA concentrations in plasma from *db*/*db* mice as well as HFD-fed obese mice than in their respective controls, whereas no EDA immunoreactivity was detected in the plasma of *Eda*-deficient *Tabby* mice[10], validating the specific detection of EDA protein in this assay (**Fig. 1i**). Analyses using an independent AlphaLISA-based immunoassay[11] further confirmed a higher abundance of circulating EDA in the plasma of *db*/*db* mice as compared to lean *misty*/*misty* control mice (**Supplementary Fig. 2b**,**c**).

To investigate whether the obesity-induced upregulation of hepatic *Eda* expression in mice was conserved in humans, we analyzed *EDA* expression in human liver samples. In a cohort of men ranging in body mass index (BMI) from 23 to 46 kg/m^2 (**Supplementary Table 4a**), liver *EDA* expression was positively correlated with visceral fat area (**Fig. 2a**) and liver fat content (**Fig. 2b**), but not with subcutaneous fat area (**Fig. 2c**) or BMI (**Supplementary Fig. 3a**). These results indicate that *EDA* expression is positively correlated with visceral adiposity rather than higher BMI, which represents a more indirect predictor of visceral adiposity (**Supplementary Fig. 3b**,**c**). Moreover, liver *EDA* expression had a negative correlation with the glucose infusion rate (GIR) in these subjects, as determined through hyperinsulinemic–euglycemic clamp studies (**Fig. 2d**). Histologically determined nonalcoholic steatohepatitis (NASH) scores for inflammation and steatosis were also positively correlated with *EDA* expression in liver (**Fig. 2e**,**f**). Finally, in another cohort of morbidly obese individuals who underwent two-step bariatric surgery intervention, liver *EDA* expression was significantly reduced 12 months after the first surgery (**Fig. 2g**) in parallel with reduction in body weight and improvement to insulin sensitivity (**Supplementary Table 4b**).

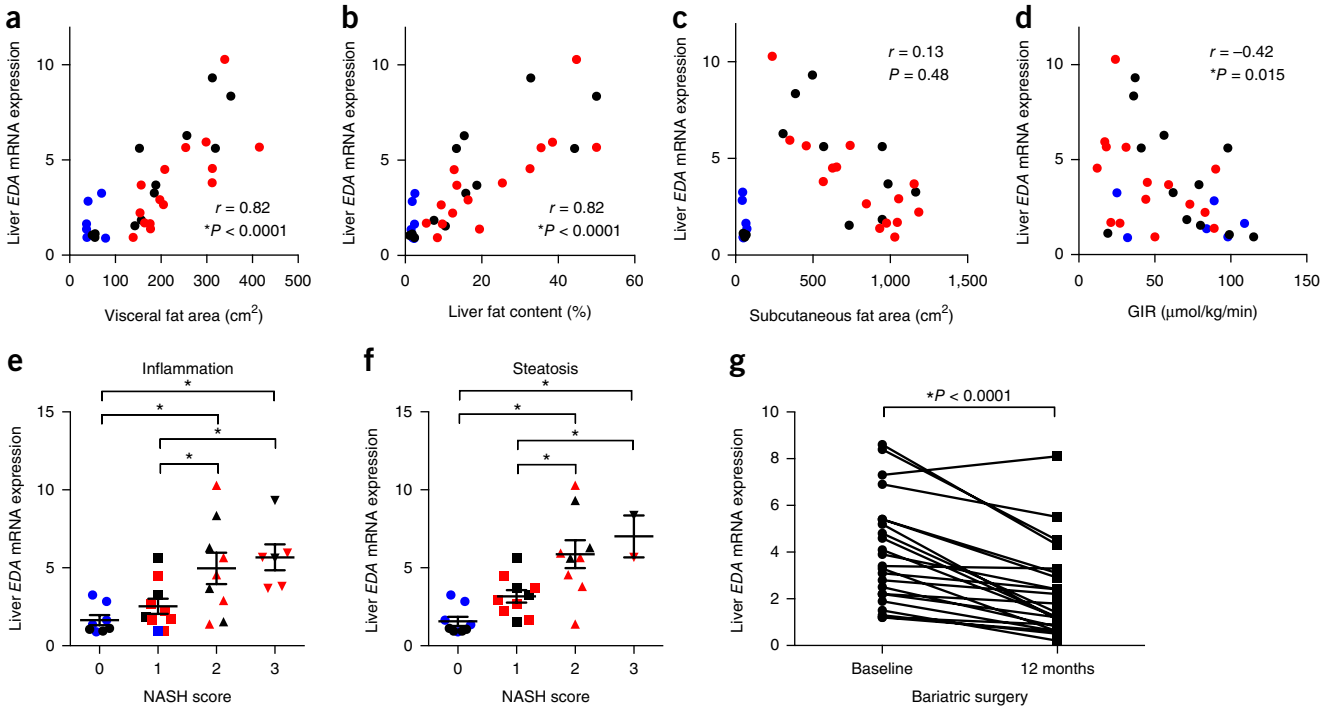

Figure 2 Increased hepatic *EDA* expression in human obesity. (**a**–**d**) Correlation of liver *EDA* mRNA expression with visceral fat area (**a**), liver fat content (**b**), subcutaneous fat area (**c**) and GIR as determined by hyperinsulinemic–euglycemic clamp studies (**d**) in a cohort of men ranging in BMI from 23 to 46 km/m^2 ($n = 33$). (**e**,**f**) Liver *EDA* expression in the cohort of men ranging in BMI from 23 to 46 km/m^2 stratified by NASH scores ($n = 33$) pertaining to inflammation (**e**) and steatosis (**f**). In **a**–**f**, blue symbols represent lean subjects (BMI < 25 kg/m^2), black symbols represent overweight subjects (25 kg/m^2 ≤ BMI < 30 kg/m^2) and red symbols represent obese subjects (BMI ≥ 30 kg/m^2) according to World Health Organization criteria. (**g**) Liver *EDA* expression in obese individuals before and 12 months after bariatric surgery ($n = 23$). Significance was determined by Spearman's correlation in **a**–**d**; one-way ANOVA with Holm–Sidak multiple-comparisons test in **e** and **f**; and a non-parametric Wilcoxon matched-pairs signed-rank test in **g**, as a normal distribution was not assumed: $^*P < 0.05$. In **e** and **f**, the graphs show mean ± s.e.m.

Next, we investigated the mechanism(s) through which obesity induces an increase in hepatic *Eda* expression. By using a *cis*-regulatory element search algorithm[12,13], we identified putative *cis*-regulatory elements for nuclear factor (NF)-κB, forkhead box O 1 (FOXO1) and peroxisome proliferator-activated receptor γ (PPARγ) in a 2.8-kb segment of the 5′ flanking region of mouse *Eda* containing the putative *Eda* promoter (**Fig. 3a**). We used this segment for subsequent promoter reporter assays in Hepa 1-6 cells. When analyzing the candidate regulatory transcription factors, only combined overexpression of PPARγ and retinoid X receptor (RXR)-α induced activity of the *Eda* promoter (**Fig. 3b**). This regulation depended on PPARγ transcriptional activity, as overexpression of a mutated PPARγ variant defective in transactivation (PPARγ E499Q)[14] failed to increase activity of the *Eda* promoter (**Fig. 3b**). On the other hand, overexpressing a constitutively nuclear form of FOXO1 (FOXO-ADA) resulted in lower activity of the *Eda* promoter (**Fig. 3b**). Among mutant reporter gene constructs for the *Eda* promoter from which the four putative PPAR-response elements (PPREs) were sequentially removed by 5′ deletion, deletion of PPRE2 reduced the reporter gene activity, as did point mutation of this PPRE in the context of the full-length promoter (**Fig. 3c**–**f**). PPARγ and RXR-α overexpression also led to an induction of *Eda* mRNA expression in Hepa 1-6 cells, which was reduced by substituting wild-type PPARγ with PPARγ E499Q (**Fig. 3g**). Furthermore, in a publically available data set for livers from mice fed on a normal or HFD (Gene Expression Omnibus (GEO), GSE55581), formaldehyde-assisted isolation of regulatory elements combined with sequencing (FAIRE–seq) analyses showed an increase in peak signal intensity in a segment located 2 to 2.5 kb upstream of the transcriptional start site (TSS) of *Eda* appearing in response to HFD (**Supplementary Fig. 4a**, upper four tracks) together with an enrichment of monomethylation of histone H3 at lysine 4 (H3K4me1) up to 2.5 kb upstream of *Eda* as determined by chromatin immunoprecipitation coupled with sequencing (ChIP–seq) (**Supplementary Fig. 4a**, lower four tracks). These data indicate that a HFD results in an increase in open chromatin in the 0.5-kb region located 2 kb upstream of the *Eda* gene in mouse liver in the context of H3K4me1 enrichment, suggesting that the PPRE2 site identified in the promoter analyses and located in this region could also serve as a regulatory element under the HFD-fed condition *in vivo*. However, overexpression of PPARγ alone did not induce activity of the *Eda* promoter but did increase the activity of the PPRE-containing control promoter (**Fig. 3b**). Likewise, treatment of *db*/*db* mice for 2 d with rosiglitazone, a glucose-lowering drug with a PPARγ-activating property, failed to further increase hepatic *Eda* mRNA expression while inducing expression of other typical target genes for PPARγ (**Supplementary Fig. 4b**,**c**). Collectively, our results highlight the potential role of combined PPARγ and RXR-α activation in fatty liver[15,16] in the regulation of hepatic *Eda* expression, whereas isolated overexpression or pharmacological activation of PPARγ does not induce hepatic *Eda* expression.

To investigate the importance of miR-676 upregulation in the livers of obese mice, we suppressed miR-676 expression in *db*/*db* mice by administrating miR-676-specific locked nucleic acid (LNA-miR-676) for 2 weeks. We found that this inhibition had no substantial

impact on glucose metabolism (**Supplementary Fig. 5a–d**). MiRNAs are known to have an impact on a broad range of target proteins and in many instances affect protein expression only to a modest degree in specific signaling networks[17,18]. Therefore, in order to characterize the impact of miR-676 suppression on the hepatic proteome in an unbiased manner, we performed *in vivo* stable isotope labeling of

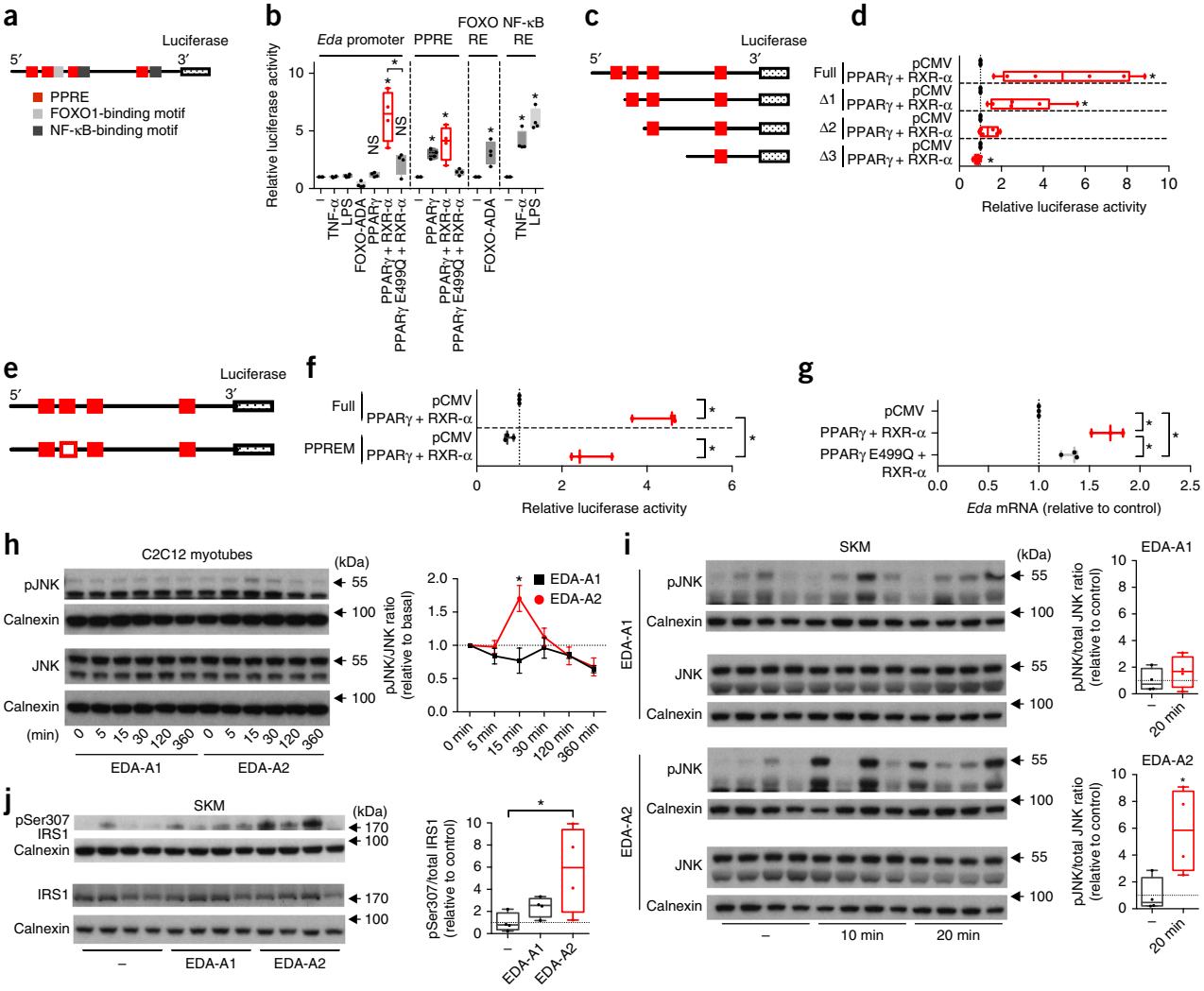

Figure 3 PPARγ and RXR-α activity promotes *Eda* transcription in hepatocytes, which in turn can activate JNK and lead to Ser307 phosphorylation of IRS1 in skeletal muscle. (**a**) Schematic of the luciferase reporter construct containing the putative *Eda* promoter region. (**b**) Promoter activity as determined by luciferase assay using the *Eda* promoter construct and treatment with the indicated stimuli or overexpression of the indicated transcription factors. As positive controls for the candidate transcription factors, reporter constructs containing a PPRE, FOXO-response element (FOXO RE) or NF-κB-response element (NF-κB RE) were employed; LPS, lipopolysaccharide. Results represent the mean of four independent experiments, each performed in quadruplicate. (**c**,**d**) Schematic of the mutant luciferase constructs with deletions in the *Eda* promoter region (Δ1–Δ3) and the full-length *Eda* promoter construct (Full) (**c**) and activity of these constructs in response to overexpression of PPARγ and RXR-α (**d**). Results represent the mean of six independent experiments, each performed in quadruplicate. (**e**,**f**) Schematic of the luciferase construct with a mutated PPRE2 site in the *Eda* promoter (PPRE M) (**e**) and the activity of this construct in response to overexpression of PPARγ and RXR-α (**f**). Results represent the mean of three independent experiments, each performed in quadruplicate. (**g**) *Eda* mRNA expression in Hepa 1-6 cells upon overexpression of wild-type or mutated PPARγ with RXR-α. Results represent the mean of three independent experiments, each performed at least in triplicate. (**h**) Immunoblots of phosphorylated JNK (pJNK), JNK and calnexin in C2C12 myotubes stimulated with recombinant EDA-A1 or EDA-A2 (left) and quantification of the ratio of phosphorylated JNK to total JNK (right). The blots are representative of four independent experiments, which were used for quantification with $n = 4$ at each time point. (**i**) Immunoblots of pJNK, JNK and calnexin in hind leg skeletal muscle (gastrocnemius + soleus) from wild-type mice injected with recombinant EDA-A1 or EDA-A2 (left) and quantification of the ratio of phosphorylated JNK to total JNK (right) ($n = 4$ under each condition). (**j**) Immunoblots of IRS1 phosphorylated at Ser307 (pSer307), IRS1 and calnexin in hind leg skeletal muscle (gastrocnemius + soleus) from wild-type mice at 20 min after injection of recombinant EDA-A1 or EDA-A2 (left) and quantification of the ratio of phosphorylated IRS1 to total IRS1 (right) ($n = 4$ under each condition). Significance was determined by repeated-measures one-way ANOVA with Holm–Sidak multiple-comparisons test with comparison to untreated controls or for the indicated pairs in **b** and **f**–**h**; a paired, two-tailed Student's *t*-test as compared to the basal condition in **d**; an unpaired, two-tailed Student's *t*-test in comparison to the basal condition in **i**; and one-way ANOVA with Holm–Sidak multiple-comparisons test in **j**: $^*P < 0.05$; NS (not significant), $P > 0.05$. For box-and-whisker plots: perimeters, 25th–75th percentile; midline, median; whiskers, minimum to maximum values; individual data points are represented. In **h**, the data are shown as mean ± s.e.m. Reporter activity and gene expression are presented as relative values normalized to the mean of the control condition, under which a control empty vector (pCMV) was transfected. Protein expression is presented as a relative value normalized to the mean of the control condition.

amino acids (SILAC) for quantitative mass spectrometry–based analysis. The SILAC-based proteomic approach enabled us to quantify more than 6,800 proteins, of which approximately 1% showed a difference of more than 1.5-fold ($P < 0.05$) in their levels in the liver of *db*/*db* mice injected with LNA-miR-676 as compared to mice injected with control LNA. Using a 1D enrichment approach that allows for detection of regulated proteins of distinct pathways[19], we found that fatty acid oxidation–related proteins were significantly upregulated, whereas complement activation– and acute-phase response–related proteins were significantly downregulated, in the livers of LNA-miR-676-injected mice as compared to mice injected with control LNA (false discovery rate (FDR) cutoff of 2%; **Supplementary Fig. 5e**). Pathway analyses using DAVID bioinformatics resources[20] confirmed the enrichment of fatty acid metabolism–related proteins among the group of proteins upregulated upon LNA-miR-676 administration (**Supplementary Fig. 5f**). These data point to the possibility that miR-676 upregulation could suppress fatty acid oxidation and further promote lipid accumulation while at the same time activating inflammatory pathways in fatty liver. However, these hypotheses need to be further validated in the future, i.e., through identification of the bona fide targets of miR-676.

We then aimed to examine the functional role of the *Mir676* host gene *Eda* in the control of metabolic homeostasis. In humans, *EDA* is a causal gene for XLHED (MIM 305100), a disorder that comprises rudimentary teeth and absence of sweat glands and hair[5]. Alternative splicing of the *EDA* transcript produces different isoforms, of which EDA-A1 and EDA-A2 are dominant[21]. EDA-A1 and EDA-A2 differ by two amino acids and bind to specific receptors, EDAR and XEDAR, respectively[22]. The previously known functions for EDA were largely limited to those of EDA-A1 in skin development; the function of EDA in adults and, in particular, the biological role of EDA-A2 have remained obscure[23]. Therefore, we next investigated whether these two EDA isoforms could be differentially regulated in obesity. Isoform-specific RT–PCR analyses showed comparable upregulation of the two isoforms in the livers of obese mouse models as compared to respective controls (**Supplementary Fig. 6a**). Notably, although the receptors for these isoforms also showed a similar expression pattern in multiple tissues of lean wild-type mice, the most abundant expression of the receptors was detected in skeletal muscle, in which *Eda2r* (*Xedar*) expression was particularly enriched (**Supplementary Fig. 6b**).

These data suggest that the EDA produced through higher expression and release from hepatocytes under conditions of obesity might act on skeletal muscle as its main target tissue. Indeed, when we stimulated cultured C2C12 mouse myotubes with recombinant EDA-A1 or EDA-A2, only EDA-A2 transiently promoted c-Jun N-terminal kinase (JNK) phosphorylation (**Fig. 3h**). EDA-A2 administration *in vivo* increased JNK phosphorylation and inhibitory phosphorylation at Ser307 of insulin receptor substrate 1 (IRS1), one of the direct mediators of the insulin-desensitizing effects of JNK[24], in muscle, whereas EDA-A1 increased phosphorylation of these proteins only marginally under the same conditions (**Fig. 3i**,**j**). In contrast, and in accordance with receptor distributions, neither EDA isoform induced JNK phosphorylation in cultured primary hepatocytes or in liver *in vivo* (**Supplementary Fig. 7**). These data are consistent with a previous report describing muscle degeneration, plausibly occurring through XEDAR-dependent inflammation, in transgenic mice expressing EDA-A2 [25].

Inflammation has long been established as a component of diabetes pathogenesis[9], in which JNK is also reported to contribute to insulin resistance in skeletal muscle[26,27]. On the other hand, we have previously reported that mice overexpressing constitutively active JNK in skeletal muscle ($JNK^{SM\text{-}C}$ mice) show no alteration in metabolic parameters upon being fed a normal chow diet under lean conditions[28]. Therefore, to further clarify the potential role of JNK in skeletal muscle in metabolic regulation under conditions of obesity, we exposed control and $JNK^{SM\text{-}C}$ mice to a HFD. On the HFD, $JNK^{SM\text{-}C}$ mice exhibited slightly increased body weight as compared to control littermates at a young age, whereas prolonged HFD negated this body weight difference between the genotypes (**Supplementary Fig. 8a**). In metabolic assessment of these animals at 8–10 weeks of age, $JNK^{SM\text{-}C}$ mice exhibited a tendency toward decreased energy expenditure, while there were no differences in locomotor activity or food intake between the genotypes (**Supplementary Fig. 8b–d**). $JNK^{SM\text{-}C}$ mice also had higher glucose levels than control littermates in a glucose tolerance test, whereas no difference between the groups was observed in blood glucose concentrations in an insulin tolerance test (**Supplementary Fig. 8e–g**). These data indicate that JNK overactivation in skeletal muscle can accelerate glucose intolerance in obesity, plausibly through interaction with other obesity-related factors, thus implying that EDA-dependent JNK activation in skeletal muscle may contribute to impaired glucose metabolism in obesity.

Next, to directly assess the impact of *Eda* upregulation on control of glucose metabolism in obesity, we first overexpressed *Eda* in the livers of mice via adeno-associated virus (AAV)-mediated gene transfer. Considering that only EDA-A2 significantly induced JNK phosphorylation in muscle, we created an AAV construct encoding mouse EDA-A2 with a Flag tag under the control of the transthyretin (*Ttr*) promoter for hepatocyte-specific overexpression of EDA-A2 (EDA-A2-AAV). We first confirmed that injection of EDA-A2-AAV into C57BL/6 mice led to release of Flag-tagged EDA protein into the circulation up to 15 weeks after injection (**Fig. 4a**). We then injected EDA-A2-AAV or control GFP-AAV into C57BL/6 mice that were fed a HFD. mRNA expression analyses in these animals showed specific overexpression of *Eda-A2* mRNA in the liver of EDA-A2-AAV-injected mice as compared to mice injected with control GFP-AAV (**Fig. 4b**). The metabolic characteristics of mice overexpressing EDA-A2 in the liver were similar to those of $JNK^{SM\text{-}C}$ mice upon HFD exposure: at 6 weeks following AAV injection and 10 weeks on a HFD, EDA-A2-AAV-injected mice exhibited higher glucose concentrations in a glucose tolerance test than control GFP-AAV-injected mice, whereas no difference was observed between these groups in the blood glucose concentrations in an insulin tolerance test (**Fig. 4c**,**d**). EDA-A2-AAV-injected mice also showed a tendency toward decreased energy expenditure without a significant difference in body weight, locomotor activity or food intake as compared to control-injected mice (**Fig. 4e–h**). Immunoblot analyses showed a higher level of JNK phosphorylation with comparable upregulation of IRS1 phosphorylation at Ser307 in the skeletal muscle (**Fig. 4i**), but not in the liver (**Supplementary Fig. 9**), of EDA-A2-AAV-injected mice as compared to control GFP-AAV-injected mice.

Next, we aimed to suppress *Eda* expression in the livers of *db*/*db* mice by delivering *Eda*-targeting short hairpin RNA (shRNA) via AAV (sh*Eda*-AAV) of the DJ/8 serotype, which is a high-affinity serotype for hepatocytes[29]. Although we minimized the AAV dose to avoid shRNA virus–related toxicity[30], sh*Eda*-AAV injection in *db*/*db* mice significantly suppressed *Eda-A1* and *Eda-A2* mRNA levels in liver (**Fig. 4j**) and consequently led to lower EDA concentrations in plasma (**Fig. 4k**) as compared to mice that were injected with control AAV encoding scrambled shRNA (shScr). Lower hepatic *Eda* expression

and circulating EDA concentrations in sh*Eda*-AAV-injected *db*/*db* mice translated into lower blood glucose concentrations in an insulin tolerance test as compared to shScr-injected control *db*/*db* mice (**Fig. 4l**) without improving the glucose tolerance of these mice (**Fig. 4m**). sh*Eda*-AAV-mediated *Eda* suppression did not affect body weight, energy expenditure, locomotor activity or food intake (**Fig. 4n–q**),

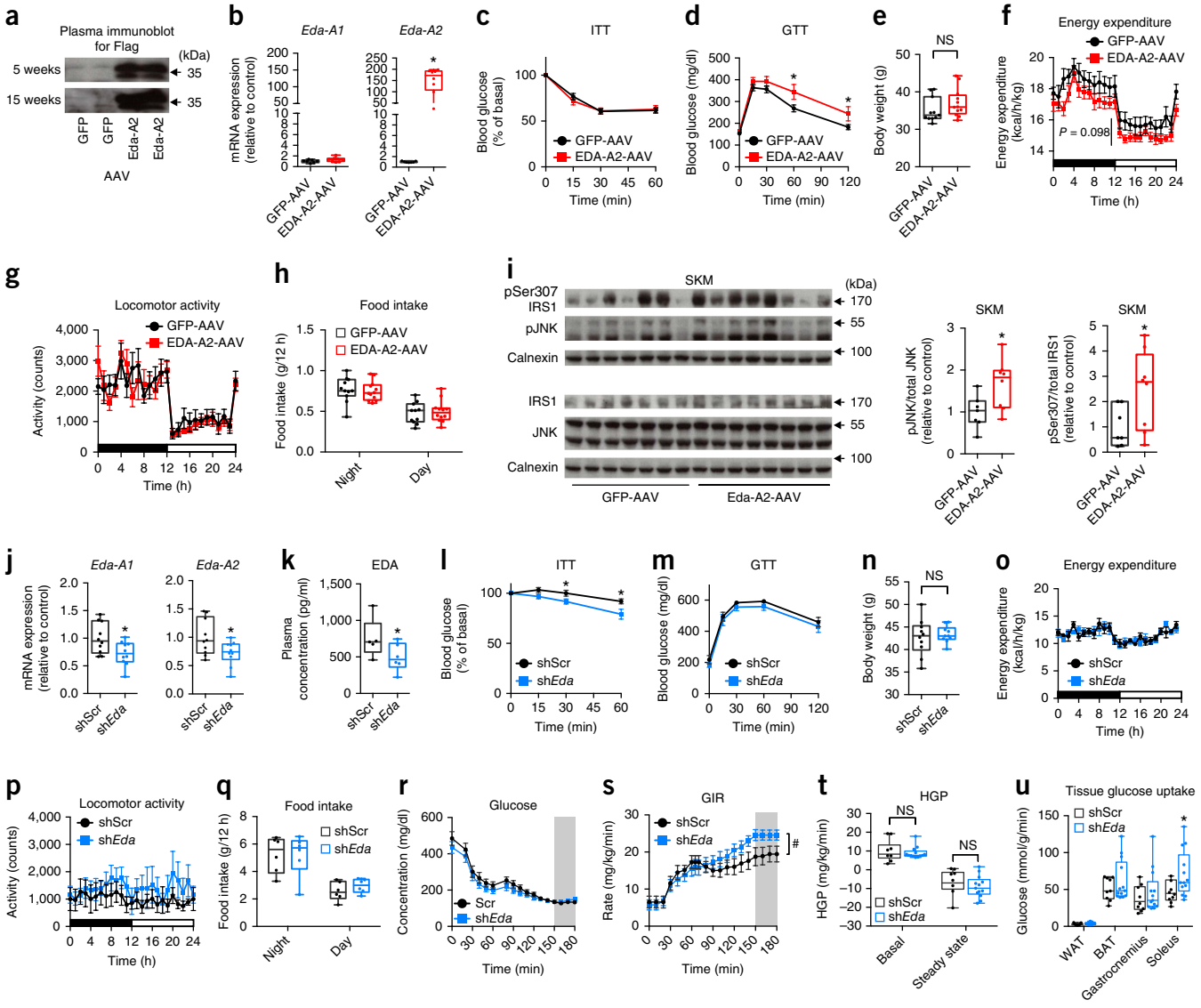

Figure 4 EDA-A2 overexpression in wild-type mice accelerates HFD-induced glucose intolerance, whereas *Eda* suppression in *db*/*db* mice ameliorates insulin resistance. (**a**) Immunoblot analysis of plasma for Flag-tagged EDA at 5 and 15 weeks after injection of control GFP-AAV or EDA-A2-AAV into C57BL/6 mice fed a NCD ($n = 2$ for both groups). (**b**–**h**) Characterization of HFD-fed C57BL/6 mice after injection with control GFP-AAV or EDA-A2-AAV. Mice were characterized for liver mRNA expression of *Eda-A1* and *Eda-A2* at 10 weeks (GFP-AAV, $n = 7$; EDA-A2-AAV, $n = 8$) (**b**); average blood glucose concentrations during an insulin tolerance test (ITT) at 6 weeks (**c**) and a glucose tolerance test (GTT) at 7 weeks (**d**) (GFP-AAV, $n = 11$; EDA-A2-AAV, $n = 12$); body weight at 7 weeks (**e**); and calorimetric measurements including energy expenditure (**f**), locomotor activity (**g**) and food intake (**h**) at 5 weeks (GFP-AAV, $n = 11$; EDA-A2-AAV, $n = 12$). On the *x* axis in **f** and **g**: black bar, darkness; white bar, light. (**i**) Immunoblots of IRS1 phosphorylated at Ser307, IRS1, pJNK, JNK and calnexin in soleus muscle at 10 weeks after injection of control GFP-AAV ($n = 7$) or EDA-A2-AAV ($n = 8$) into HFD-fed C57BL/6 mice (left) and quantification (right). (**j**–**q**) Metabolic characterization of *db*/*db* mice injected with control shScr-AAV or sh*Eda*-AAV. Mice were characterized for liver mRNA expression of *Eda-A1* and *Eda-A2* ($n = 10$ for both groups) (**j**); plasma EDA concentrations (shScr-AAV, $n = 5$; sh*Eda*-AAV, $n = 6$) (**k**); average blood glucose concentrations during an insulin tolerance test (**l**) and a glucose tolerance test (**m**) ($n = 10$ for both groups); body weight ($n = 10$ for both groups) (**n**); and calorimetric measurements including energy expenditure (**o**), locomotor activity (**p**) and food intake (**q**) ($n = 6$ for both groups). On the *x* axis in **o** and **p**: black bar, darkness; white bar, light. (**r**–**u**) Analyses of a hyperinsulinemic–euglycemic clamp experiment in which *db*/*db* mice were injected with control shScr-AAV ($n = 10$) or sh*Eda*-AAV ($n = 13$). Mice were analyzed for glucose levels (**r**) and GIR (**s**), hepatic glucose production (HGP) (**t**) and glucose uptake in the indicated tissues (**u**). Significance was determined by unpaired, two-tailed Student's *t*-test in comparison to control mice in **b**, **d**, **e**, **i**, **j**, **l**, **n**, **t** and **u**; two-way ANOVA in **f**; an unpaired, one-tailed Student's *t*-test performed based on the predicted reduction in EDA in sh*Eda*-AAV-injected mice in **k**; and two-way ANOVA applied for the GIR after the mice reached the steady state (120–150 min) in **s**: $*P < 0.05$, $\#P < 0.05$ between the shScr-AAV and sh*Eda*-AAV groups; NS, $P > 0.05$. For box-and-whisker plots: perimeters, 25th–75th percentile; midline, median; whiskers, minimum to maximum values; individual data points are represented. In **c**, **d**, **f**, **g**, **l**, **m**, **o**, **p**, **r** and **s**, the data are shown as mean ± s.e.m. Gene and protein expression are presented as relative values normalized to the mean of the controls.

indicating that suppression of hepatic *Eda* expression in obese mice ameliorated insulin resistance through direct effects on target tissues for peripheral insulin. In accordance with the improved insulin sensitivity in sh*Eda*-AAV-injected *db*/*db* mice, in hyperinsulinemic–euglycemic clamp studies, we observed a significantly higher GIR in these mice (**Fig. 4r**,**s**), associated with increased glucose uptake in soleus muscle, whereas suppression of hepatic glucose production did not differ relative to shScr-injected control *db*/*db* mice (**Fig. 4t**,**u**).

RNA-seq analyses of RNA isolated from soleus muscle in sh*Eda*-AAV-injected *db*/*db* mice identified 289 genes upregulated and 442 genes downregulated (fold change ≥ 1.2, $P < 0.05$) in comparison to shScr-AAV-injected mice. Pathway analyses[20] found significant enrichment of genes implicated in glycolysis and insulin signaling among the upregulated genes (**Supplementary Fig. 10**), further supporting the notion of enhanced insulin sensitivity in muscle[31], whereas cardiomyopathy-related genes were enriched among the downregulated genes.

Taken together, our results provide evidence that deregulated hepatic expression of *Eda*, particularly the *Eda-A2* isoform, contributes to obesity-associated deterioration of insulin sensitivity in muscle and glucose homeostasis and that the similarly upregulated miR-676 acts as a potential negative regulator of fatty acid oxidation in liver. The protein encoded by *EDA*, a causal gene in XLHED, was previously known to regulate skin appendage formation during development, but the biological role in adults of EDA, especially the EDA-A2 isoform, has been poorly understood[5,25,32]. In our study, we observed obesity-associated increases in hepatic *EDA* expression in obese male human subjects that were correlated with features of insulin resistance and found that increased *EDA* levels were reversed upon successful weight loss. Our gene regulation experiments indicate that hepatic steatosis may promote *Eda* expression in a PPARγ- and RXR-α-dependent manner. This idea is consistent with the correlation of hepatic *EDA* expression with clinical NASH scores in humans. Finally, our experiments characterize EDA as a hepatokine that contributes to the impaired sensitivity to systemic insulin found in obesity primarily by acting on skeletal muscle. This EDA-mediated insulin resistance could plausibly involve inflammatory pathway activation, although other mechanisms in addition to JNK activation still need to be investigated in the future.

Furthermore, given the well-defined role of EDA in skin homeostasis, it is tempting to speculate that the increased amount of circulating EDA under conditions of obesity could cause functional changes in skin homeostasis[33,34]. Skin appendage physiology has thus far been underinvestigated in the context of metabolic disorders. However, associations of nutritional status with sebum production[35,36] and eccrine gland activity[37] have long been described, and individuals with XLHED often have unexplained low body weights without defects in caloric intake or absorption[38,39]. The present study provides a potential molecular link between skin appendage function and metabolism, which awaits additional research. Further, soluble EDA or its receptor may represent a possible pharmacological target for improvement of insulin sensitivity in type 2 diabetes, although, given the modest effects in the *db*/*db* mouse model, further exploration of the pathway will be required.

METHODS

Methods, including statements of data availability and any associated accession codes and references, are available in the online version of the paper.

Note: Any Supplementary Information and Source Data files are available in the online version of the paper.

ACKNOWLEDGMENTS

We acknowledge J. Alber, B. Hampel, P. Scholl, N. Spenrath and D. Kutyniok for outstanding technical assistance. We greatly appreciate P. Schneider (Lausanne University) for providing *Tabby* mice and EDA expression vectors as well as outstanding support in performance of the EDA AlphaLISA assay. We acknowledge J. Wilson (University of Pennsylvania) for providing the pXR8 plasmid and J. Samulski (University of North Carolina) for providing the pXX6-80 plasmid. We acknowledge P. Frommolt for bioinformatics support and H. Büning for support of AAV production. This work was supported by a grant from the German Research Foundation (DFG) (BR 1492/7-1) to J.C.B., and we received funding from DFG within the framework of TRR134 and within the Excellence Initiative by German Federal and State Governments (CECAD). This work was funded (in part) by the Helmholtz Alliance (Imaging and Curing Environmental Metabolic Diseases, ICEMED) through the Initiative and Networking Fund of the Helmholtz Association. J.W.K. greatly appreciates funding from the Emmy Noether program of DFG (KO 4728/1-1). M.A. gratefully acknowledges support from a Manpei Suzuki Diabetes Foundation fellowship.

AUTHOR CONTRIBUTIONS

M.A. and J.C.B. designed the study and wrote the manuscript. M.A. and P.G. performed experiments, and M.A. analyzed data. E.T. performed the surgeries and with P.G. conducted the hyperinsulinemic–euglycemic clamp experiment. C.B. also supported the hyperinsulinemic–euglycemic clamp studies. H.N. and M.K. performed SILAC and proteomic analyses. P.J.A. contributed to AAV generation. J.S. provided critical reagents. J.A. performed miRNA sequencing, and S.M. analyzed the data. F.T.W. provided JNK^{SM-C} mice. J.-W.K. provided the microarray data. M.B. provided the human samples and clinical data.

COMPETING FINANCIAL INTERESTS

The authors declare no competing financial interests.

1. Davis, B.N. & Hata, A. Regulation of microRNA biogenesis: a miRiad of mechanisms. *Cell Commun. Signal.* **7**, 18 (2009).
2. Gromak, N. Intronic microRNAs: a crossroad in gene regulation. *Biochem. Soc. Trans.* **40**, 759–761 (2012).
3. Najafi-Shoushtari, S.H. *et al.* MicroRNA-33 and the SREBP host genes cooperate to control cholesterol homeostasis. *Science* **328**, 1566–1569 (2010).
4. Ma, N. *et al.* Coexpression of an intronic microRNA and its host gene reveals a potential role for miR-483-5p as an IGF2 partner. *Mol. Cell. Endocrinol.* **333**, 96–101 (2011).
5. Mikkola, M.L. Molecular aspects of hypohidrotic ectodermal dysplasia. *Am. J. Med. Genet. A.* **149A**, 2031–2036 (2009).
6. Kornfeld, J.W. *et al.* Obesity-induced overexpression of miR-802 impairs glucose metabolism through silencing of *Hnf1b*. *Nature* **494**, 111–115 (2013).
7. Mikkola, M.L. *et al.* Ectodysplasin, a protein required for epithelial morphogenesis, is a novel TNF homologue and promotes cell-matrix adhesion. *Mech. Dev.* **88**, 133–146 (1999).
8. Schneider, P. *et al.* Mutations leading to X-linked hypohidrotic ectodermal dysplasia affect three major functional domains in the tumor necrosis factor family member ectodysplasin-A. *J. Biol. Chem.* **276**, 18819–18827 (2001).
9. Hotamisligil, G.S., Shargill, N.S. & Spiegelman, B.M. Adipose expression of tumor necrosis factor-α: direct role in obesity-linked insulin resistance. *Science* **259**, 87–91 (1993).
10. Srivastava, A.K. *et al.* The Tabby phenotype is caused by mutation in a mouse homologue of the *EDA* gene that reveals novel mouse and human exons and encodes a protein (ectodysplasin-A) with collagenous domains. *Proc. Natl. Acad. Sci. USA* **94**, 13069–13074 (1997).
11. Podzus, J. *et al.* Ectodysplasin A in biological fluids and diagnosis of ectodermal dysplasia. *J. Dent. Res.* **96**, 217–224 (2017).
12. Messeguer, X. *et al.* PROMO: detection of known transcription regulatory elements using species-tailored searches. *Bioinformatics* **18**, 333–334 (2002).
13. Farré, D. *et al.* Identification of patterns in biological sequences at the ALGGEN server: PROMO and MALGEN. *Nucleic Acids Res.* **31**, 3651–3653 (2003).
14. Hauser, S. *et al.* Degradation of the peroxisome proliferator-activated receptor γ is linked to ligand-dependent activation. *J. Biol. Chem.* **275**, 18527–18533 (2000).
15. Vidal-Puig, A. *et al.* Regulation of PPARγ gene expression by nutrition and obesity in rodents. *J. Clin. Invest.* **97**, 2553–2561 (1996).
16. Pettinelli, P. & Videla, L.A. Up-regulation of PPAR-γ mRNA expression in the liver of obese patients: an additional reinforcing lipogenic mechanism to SREBP-1c induction. *J. Clin. Endocrinol. Metab.* **96**, 1424–1430 (2011).
17. Baek, D. *et al.* The impact of microRNAs on protein output. *Nature* **455**, 64–71 (2008).

18. Selbach, M. *et al*. Widespread changes in protein synthesis induced by microRNAs. *Nature* **455**, 58–63 (2008).
19. Cox, J. & Mann, M. 1D and 2D annotation enrichment: a statistical method integrating quantitative proteomics with complementary high-throughput data. *BMC Bioinformatics* **13**Suppl 16, S12 (2012).
20. Huang, W., Sherman, B.T. & Lempicki, R.A. Systematic and integrative analysis of large gene lists using DAVID bioinformatics resources. *Nat. Protoc.* **4**, 44–57 (2009).
21. Hashimoto, T., Cui, C.Y. & Schlessinger, D. Repertoire of mouse ectodysplasin-A (EDA-A) isoforms. *Gene* **371**, 42–51 (2006).
22. Yan, M. *et al*. Two–amino acid molecular switch in an epithelial morphogen that regulates binding to two distinct receptors. *Science* **290**, 523–527 (2000).
23. Lindfors, P.H., Voutilainen, M. & Mikkola, M.L. Ectodysplasin/NF-κB signaling in embryonic mammary gland development. *J. Mammary Gland Biol. Neoplasia* **18**, 165–169 (2013).
24. Copps, K.D. & White, M.F. Regulation of insulin sensitivity by serine/threonine phosphorylation of insulin receptor substrate proteins IRS1 and IRS2. *Diabetologia* **55**, 2565–2582 (2012).
25. Newton, K., French, D.M., Yan, M., Frantz, G.D. & Dixit, V.M. Myodegeneration in EDA-A2 transgenic mice is prevented by XEDAR deficiency. *Mol. Cell. Biol.* **24**, 1608–1613 (2004).
26. Hirosumi, J. *et al*. A central role for JNK in obesity and insulin resistance. *Nature* **420**, 333–336 (2002).
27. Sabio, G. *et al*. Role of muscle c-Jun NH_2-terminal kinase 1 in obesity-induced insulin resistance. *Mol. Cell. Biol.* **30**, 106–115 (2010).
28. Pal, M. *et al*. Alteration of JNK-1 signaling in skeletal muscle fails to affect glucose homeostasis and obesity-associated insulin resistance in mice. *PLoS One* **8**, e54247 (2013).
29. Grimm, D. *et al*. *In vitro* and *in vivo* gene therapy vector evolution via multispecies interbreeding and retargeting of adeno-associated viruses. *J. Virol.* **82**, 5887–5911 (2008).
30. Grimm, D. *et al*. Fatality in mice due to oversaturation of cellular microRNA/short hairpin RNA pathways. *Nature* **441**, 537–541 (2006).
31. Izumiya, Y. *et al*. Fast/glycolytic muscle fiber growth reduces fat mass and improves metabolic parameters in obese mice. *Cell Metab.* **7**, 159–172 (2008).
32. Tanikawa, C., Ri, C., Kumar, V., Nakamura, Y. & Matsuda, K. Crosstalk of EDA-A2/XEDAR in the p53 signaling pathway. *Mol. Cancer Res.* **8**, 855–863 (2010).
33. Kowalczyk-Quintas, C. *et al*. Pharmacological stimulation of Edar signaling in the adult enhances sebaceous gland size and function. *J. Invest. Dermatol.* **135**, 359–368 (2015).
34. Cui, C.Y. *et al*. Inducible mEDA-A1 transgene mediates sebaceous gland hyperplasia and differential formation of two types of mouse hair follicles. *Hum. Mol. Genet.* **12**, 2931–2940 (2003).
35. Pochi, P.E., Downing, D.T. & Strauss, J.S. Sebaceous gland response in man to prolonged total caloric deprivation. *J. Invest. Dermatol.* **55**, 303–309 (1970).
36. Chen, H.C., Smith, S.J., Tow, B., Elias, P.M. & Farese, R.V. Jr. Leptin modulates the effects of acyl CoA:diacylglycerol acyltransferase deficiency on murine fur and sebaceous glands. *J. Clin. Invest.* **109**, 175–181 (2002).
37. Yosipovitch, G., DeVore, A. & Dawn, A. Obesity and the skin: skin physiology and skin manifestations of obesity. *J. Am. Acad. Dermatol.* **56**, 901–916, quiz 917–920 (2007).
38. Fete, M., Hermann, J., Behrens, J. & Huttner, K.M. X-linked hypohidrotic ectodermal dysplasia (XLHED): clinical and diagnostic insights from an international patient registry. *Am. J. Med. Genet. A.* **164A**, 2437–2442 (2014).
39. Motil, K.J. *et al*. Growth characteristics of children with ectodermal dysplasia syndromes. *Pediatrics* **116**, e229–e234 (2005).

ONLINE METHODS

Microarray analysis of microRNAs. RNA from the livers of NCD- or HFD-fed mice and *db*/*db* mice or their controls was isolated using the mirVana miRNA Isolation Kit (Ambion, Life Technologies) following the protocol for total RNA isolation. RNA integrity and concentration were assessed using the Experion Bioanalyzer system (Bio-Rad) according to the manufacturer's instructions. MiRNA expression levels were quantified using a microfluidic card qRT–PCR system with TaqMan Array Rodent MicroRNA A+B Cards (Applied Biosystems). These arrays cover 674 murine miRNAs, including small nucleolar RNAs as appropriate controls. Real-time qPCR was run on an Applied Biosystems 7900HT Fast Real-Time System. Relative expression of mature miRNAs was determined using a comparative method as previously described[6]. To screen for dysregulated miRNAs, we selected for further analyses miRNAs that showed significantly upregulated expression in liver of *db*/*db* mice (fold change ≥ 1.5, $P < 0.1$) and increase in the liver of mice with HFD-induced obesity (fold change ≥ 1.2, regardless of *P* value) as compared to lean control mice. This analysis was based on a data set originally described in a previous report[6].

Animals. Male BKS.Cg-*Dock7*^{m} +/+ *Lepr*^{db}/J (*db*/*db*) mice and control *misty*/*misty* mice were purchased from Jackson Laboratory or Janvier Labs. We used *misty* mice as control animals, as they are the littermates of *db*/*db* mice generated on the BKS.Cg-*Dock7*^{m} +/+ *Lepr*^{db}/J background. Mice in this system can be rapidly genotyped for the *db* mutation in *Lepr* by coat color and early obesity development because the allele of *Dock7* with the recessive *misty* mutation resulting in a greyish coat color is in repulsion to the *db* allele of *Lepr*. Wild-type male C57BL/6JRj mice were purchased from Janvier Labs. *Eda*-deficient B6CBAa *A*$^{w\text{-}J}$/*A*-*Eda*^{Ta}/*J* (*Tabby*) mice were kindly provided by P. Schneider (Lausanne University). The generation of mice expressing a constitutively active version of JNK specifically in skeletal muscle (JNK$^{SM\text{-}C}$) was described previously[28]. Mice were housed at 22–24 °C in a 12-h light/12-h dark cycle and fed a standard rodent normal chow diet (Teklad Global Rodent T.2018.R12; Harlan) unless otherwise indicated. For experiments with HFD feeding, mice were assigned either a HFD (D12492, 60% kcal from fat, Research Diets) or a sucrose-matched low-fat diet (normal chow diet) (D12450 J, 10% kcal from fat, Research Diets) when applicable at 4 weeks of age. For characterization of *Eda* and miR-676 expression in liver and other tissues under HFD conditions, tissues were collected at 36 weeks of age and subjected to measurements, whereas for EDA protein expression studies liver was collected from a different cohort of mice at 12 months of age. Detailed experimental parameters for the other mouse models are provided below. All animals were randomly assigned to experimental groups, and tests were done without blinding. Sample sizes for animal experiments were assessed by power calculations with an alpha value of 0.8 and were chosen on the basis of experience in previous in-house studies of metabolic phenotypes and to balance the ability to detect significant differences with minimization of the number of animals used. All animal procedures were performed in accordance with the Directive 2010/63/EU of the European Parliament and of the Council of the European Union (issued 22 September 2010). The German Federal Ministry of Food and Agriculture issued the regulation for implementation of the Directive 2010/63/EU into German law on 1 August 2013. In accordance with these rules, our protocol was approved by the North Rhine-Westphalia State Agency for Nature, Environment and Consumer Protection; they were assisted by an animal welfare committee. Permission to maintain and breed mice was issued by the Department for Environment and Consumer Protection–Veterinary Section, Cologne, North Rhine-Westphalia, Germany. All animal procedures were performed in accordance with National Institutes of Health guidelines.

Real-time qPCR. Total RNA was prepared using the mirVana miRNA Isolation Kit (Life Technologies). cDNA was prepared using Reverse Transcription Reagents (Life Technologies). Real-time qPCR was performed with QuantiStudio 7 Flex (Life Technologies) using TaqMan Real Time PCR Master Mix Reagent (Life Technologies). Expression of the two different EDA isoforms was quantified by real-time qPCR with SYBR Green Master Mix Reagent (Life Technologies) using specific primer pairs distinguishing *Eda-A1* and *Eda-A2*: *Eda-A1* and *Eda-A2* Fwd, 5-AACAACTGTTATGGGACCAC-3; *Eda-A1* Rev, 5-TGAAGTTGATGTAGTAGACTTC-3; *Eda-A2* Rev, 5-TGA AGTTGATGTAGTAGACCTG-3. All other real-time qPCR assays were performed with TaqMan Gene Expression Assays (Applied Biosystems). Relative gene expression was calculated by a comparative method using values normalized to the expression of an internal control gene.

Northern blotting. A miR-676-specific LNA probe was purchased from Exiqon. Total RNA was prepared with the mirVana miRNA Isolation Kit (Life Technologies), and 15 µg of RNA was separated by electrophoresis followed by semidry transfer at 4 mA/cm^2 for 45 min onto Nytran N membrane (Schleicher & Schuell). After ultraviolet (UV) cross-linking and baking at 80 °C for 30 min, the membrane was incubated with radiolabeled LNA probe overnight at 37 °C according to the manufacturer's protocol. Images were obtained with a Typhoon Scanner FLA (GE Healthcare). Images of 5.8S and 5S ribosomal RNA obtained of the gel after electrophoresis were used as loading control.

Small RNA sequencing analyses. Libraries were prepared using the Illumina TruSeq Small RNA Sample Preparation Kit. Library preparation started with 1 µg of total RNA. After ligation with 3 and 5 RNA adaptors, RT–PCR was used for first-strand synthesis. Fragments were amplified to complete adaptor constructs and gel purified for size selection. After library validation and quantification (using an Agilent 2100 Bioanalyzer), equimolar amounts of the libraries were pooled. Pools were quantified using the Peqlab KAPA Library Quantification Kit and the Applied Biosystems 7900HT Sequence Detection System. Pools were then sequenced using an Illumina GAIIX instrument and a 1 × 37-bp read-length protocol. Adaptors were trimmed from the ends of the reads using cutadapt 1.2.1, and miRNA read counts were computed for each sample by counting the number of trimmed reads perfectly matching the known *Mus musculus* miRNA sequences from miRBase 20. Read counts were normalized to RPM (reads per million) values for each of the samples.

Hepatocyte isolation and fractionation. Mice were subjected to experiments around the age of 8 weeks. Under anesthesia, mice were perfused via the portal vein with 50 ml of perfusion medium, followed by digestion with 50 ml of collagenase medium. Dissociated cells from the liver were filtered through a cell strainer (BD Falcon) into DMEM, low glucose (Gibco) supplemented with 10% FBS and 1% penicillin–streptomycin and then were centrifuged twice at 50*g* for 3 min to recover the pellet and the supernatant. Hepatocytes were obtained by resuspending the pellet in 30% Percoll and centrifuging at 150*g* for 7 min. For the non-hepatocyte fraction, the supernatant was centrifuged at 350*g* and the resulting cell pellet was centrifuged on a 20% (w/vol) Histodenz (Sigma) gradient. For fractionation analyses, both fractions were frozen immediately after isolation and subjected to further analyses. For experiments in which hepatocytes were stimulated, cells were attached to collagen-coated plates (Costar) for 2 h and were grown in penicillin–streptomycin-supplemented DMEM, low glucose (Life Technologies) without FBS overnight; they were then subjected to stimulation on the following day. The media were as follows: perfusion medium, HBSS (Gibco) without magnesium or calcium and supplemented with 0.5 mM EGTA; collagenase medium, DMEM, low glucose (Gibco) supplemented with 15 mM HEPES and 100 collagen digestion units (CDU)/ml of collagenase, type IV (Worthington); 90% concentrated Percoll, 100% Percoll (Amersham) diluted with 10× HBSS (Gibco). Cell fractions were isolated from four *misty*/*misty* and four *db*/*db* mice. One nonparenchymal fraction of each genotype exhibited contamination as assessed by hepatocyte marker expression, and these two samples were thus excluded from further analyses.

Immunoblotting. Tissues were homogenized in liver buffer composed of 25 mM Tris-HCl, pH 7.4, 10 mM Na_3VO_4, 100 mM NaF, 50 mM $Na_4P_2O_7$, 10 mM EGTA, 10 mM EDTA and 1% Nonidet P-40 supplemented with cOmplete Mini Protease Inhibitor Cocktail (Roche). After homogenization, lysate was centrifuged at 17,000*g* for 20 min at 4 °C, and the supernatant was recovered. Protein concentration was determined using the BCA Assay Kit (Thermo Fisher Scientific) and was adjusted to 2 mg/ml. Samples for immunoblotting were prepared by heating at 95 °C with Laemmli buffer for 5 min, except for

doi:10.1038/nm.4420

those used in the anti-EDA immunoblot, which were denatured at 70 °C for 5 min to avoid aggregation of EDA. The prepared samples were subjected to SDS–PAGE using NuPAGE 4–12% Bis-Tris Precast Gels (Thermo Fisher Scientific), followed by electrical transfer onto a PVDF membrane using the Trans-Blot Turbo system (Bio-Rad). After blocking with Western Blocking Reagent (Roche), the membrane was incubated with primary antibody at 4 °C overnight. Subsequently, after incubation with secondary antibody, the blot was developed using Pierce ECL Western Blotting Substrate (Thermo Fisher Scientific). Images derived from one gel are displayed with thin intervening spaces, whereas images obtained from independent gels are separated from one another by broader intervening spaces. All densitometry measurements were performed with the Fiji image processing package. For quantification of JNK, the 54-kDa isoform was used for densitometry measurement. Band intensity was normalized to that of calnexin blotted on the same gel and membrane as the loading control; when applicable, the ratio of phosphorylated protein to total protein was calculated using these normalized values. Uncropped images for all immunoblots are displayed in **Supplementary Figure 11**.

Antibodies for immunoblotting. Antibodies against phospho-SAPK/JNK (Thr183/Thr185) (catalog no. 4668), SAPK/JNK (catalog no. 9252) and DYKDDDDK tag (catalog no. 2368; binding to the same epitope as Sigma's Anti-Flag M2 antibody) were purchased from Cell Signaling Technology and used at a 1:2,000 dilution. For the IRS1 immunoblot, anti-IRS1 antibody purchased from BD Biosciences (611395) was used at a 1:1,000 dilution, except for the experiments in **Figure 4i**, in which anti-IRS1 antibody purchased from Abcam (ab131487) was used at a 1:1,000 dilution. Anti-calnexin antibody (catalog no. 208880) was purchased from Calbiochem and used at a 1:5,000 dilution. Anti–phosphorylated IRS1 (Ser307) (ab5599) was purchased from Abcam and used at a 1:2,000 dilution. Anti-EDA-A1 mouse mAb Renzo-2 was available from Enzo Life Sciences (ALX-522-038) and used at a 1:1,000 dilution. Peroxidase-conjugated anti–rabbit IgG (A6154) and anti–mouse IgG (A4416) secondary antibodies were purchased from Sigma-Aldrich and used at a 1:5,000 dilution, except for the blot using anti-IRS1 antibody (BD Bioscience), in which the secondary antibody was used at a 1:1,000 dilution.

Cells and cell culture. Hepa 1-6 cells were cultured in DMEM supplemented with penicillin–streptomycin and 10% FBS. C2C12 cells were differentiated in DMEM supplemented with penicillin–streptomycin and 2% horse serum for 6 d and subjected to experiments. Cells were obtained from the American Type Culture Collection (ATCC) and tested negative for mycoplasma contamination. All cell culture experiments were conducted without blinding.

Secretion study of EDA. Hepa 1-6 cells were plated onto a 12-well plate at a density of 2×10^5 cells per well, and 1.6 µg of pCR3 expression vector encoding full-length human EDA-A1 or mutant human EDA-A1 R156C[8] (both kindly provided by P. Schneider, Lausanne University) or of control empty vector was transfected into cells by Lipofectamine 2000 (Life Technologies) following the manufacturer's protocol. On the following day, the medium was changed to 500 µl of serum-free medium, and cells were further incubated overnight. The cell culture medium was then collected, and cells were washed with 200 µl of PBS containing 1% heparin (pooled as the supernatant fraction) before collection. Cells were immediately frozen in liquid nitrogen. For immunoblotting, cell lysates were prepared as previously described[40] and Laemmli buffer was directly added to the supernatant fraction. 10 µl per lane of supernatant samples was loaded for SDS–PAGE.

Measurement of circulating EDA. Plasma samples were collected with heparin-coated capillaries followed by centrifugation. Plasma EDA concentrations were quantified by ELISA using the Mouse Ectodysplasin A ELISA Kit (MBS930835, MYBioSource) according to the manufacturer's recommendations, with 50 µl of plasma diluted with the supplied sample diluent buffer. Plasma concentrations of EDA were inferred from the standard curve calculated using standard sample measurements in the supplied buffer. Plasma samples from *db*/*db* mice were mixed with plasma from *Tabby* mice or sample diluent buffer at a 1:1 ratio and subjected to measurement to confirm that the failure of EDA detection in *Tabby* mouse plasma was not due to a quenching property in the plasma. In the AlphaLISA immunoassay, EDA in plasma (mock depleted or depleted on EctoD2-coated plates) was measured by AlphaLISA with anti-EDA monoclonal antibodies EctoD2 and EctoD3 and Fc-EDA1 as a standard, as described previously[11].

Characterization of human liver samples. In a first cohort, *EDA* mRNA expression was measured in liver tissue samples obtained from 33 men who underwent open abdominal surgery for Roux-en-Y bypass, sleeve gastrectomy, explorative laparotomy or elective cholecystectomy (**Supplementary Table 4a**). A small liver biopsy was taken during the surgery, immediately snap frozen in liquid nitrogen and stored at −80 °C until further preparations. All baseline blood samples and liver biopsies were collected between 8:00 a.m. and 10:00 a.m. after an overnight fast, and the visceral fat area, liver fat content, and subcutaneous fat area were determined in abdominal magnetic resonance imaging studies as described previously[41].

In addition, we included samples from 23 obese patients of European ancestry (14 women, 9 men) who underwent a two-step bariatric surgery strategy with gastric sleeve resection as the first step and Roux-en-Y gastric bypass as the second step 12 ± 2 months later (**Supplementary Table 4b**). At both time points, liver biopsies were obtained. General inclusion and exclusion criteria as well as methods for the measurement of anthropometric and laboratory parameters have been reported recently[42]. Study protocols have been approved by the ethics committee of the University of Leipzig (reg. no. 031-2006 and 017-12-23012012). All participants gave written informed consent before taking part in the study.

Human liver *EDA* mRNA expression was measured by real-time qPCR in a fluorescence thermal cycler (ABI PRISM 7000 sequence detector, Applied Biosystems, Darmstadt, Germany) using a TaqMan assay-on-demand kit (Hs03025596_s1, Applied Biosystems). *EDA* mRNA expression was calculated relative to the mRNA expression of *HPRT1*.

Promoter assays. The 2.8-kb region upstream of the mouse *Eda* gene and fragments of it derived through sequential PCRs were subcloned into the pGL4.10[luc2] vector (Promega). pGL4.32[*luc2P*/NF-κB-RE/Hygro] vector was purchased from Promega. Hepa 1-6 cells were plated onto a 24-well plate, and 100 ng of the luciferase reporter plasmid and 20 ng of a *Renilla* luciferase plasmid (pRL-null, Promega) were cotransfected into cells with a total of 600 ng of specific expression vectors by Lipofectamine 2000 (Life Technologies). At 48 h following transfection, cells were harvested and subjected to luciferase assays using the Dual-Luciferase Reporter Assay System (Promega) following the manufacturer's protocol. Where indicated, cells were stimulated with TNF (100 ng/ml) or LPS (20 µg/ml) for 6 h before harvesting. All other vectors were obtained via Addgene: pSV Sport RXR alpha (8882); Flag-FoxO1-ADA (12149); pcDNA flag PPAR gamma (8895); pcDNA flag PPAR gamma E499Q (8896).

Thiazolidinedione treatment of *db*/*db* mice. Rosiglitazone (purchased from Sigma-Aldrich) was suspended in 1% Tween-80 solution. At 8 weeks of age, 16 *db*/*db* mice were randomly divided into two groups and administered 5 mg per kg body weight of rosiglitazone or an equivalent volume of vehicle by oral gavage once per day. After 2 d of treatment, mice were euthanized and livers were collected for gene expression analyses.

Locked nucleic acid treatment of *db*/*db* mice. Custom-made miRCURY LNA miRNA inhibitor was designed and synthesized by Exiqon as a fully complementary nucleotide to the seed-containing region of mature miR-676 (LNA-miR-676, 5′-AACAACCTCAGGACG-3′).A negative control with no homology to any known mouse miRNA sequence was used as the control LNA (LNA control). *db*/*db* mice were intraperitoneally injected once per week with 5 mg per kg body weight of LNA dissolved in PBS for 2 weeks starting from 8 weeks of age and thereafter subjected to metabolic assessments. Organ collection was conducted after fasting for 6 h.

Proteomics analyses of livers from locked nucleic acid–treated db/db mice. *Protein digestion*. Livers from *db*/*db* animals treated with LNA-miR-676 (n = 4) or control LNA (n = 4) and SILAC mice[43] were crushed to powder using a mortar in liquid nitrogen and resuspended in RIPA buffer (150 mM NaCl,

0.2% sodium deoxycholate, 0.1% SDS, 50 mM Tris, pH 8.0) and then acetone precipitated for clarification. The protein pellet was dissolved in 6 M urea, 2 M thiourea in 10 mM HEPES, pH 8, and protein concentration was determined. [^{13}C]lysine-labeled proteins from SILAC mice were spiked in at a 1:1 ratio with samples serving as an internal standard. In total, 2 mg of protein was reduced by 10 mM dithiothreitol and alkylated by 55 mM iodacetamide in the dark. Then Lys-C was added at a ratio of 1:100 and samples were incubated at room temperature for at least 2 h. The urea concentration was diluted to 2 M by 50 mM ammonium bicarbonate, and Lys-C was added at the same ratio as before for overnight digestion. Digestion was stopped by adding acetonitrile (ACN) and TFA to final concentrations of 2.5% and 0.2%, respectively. Generated peptides were desalted by C18 Cartridges (Waters) and concentrated in a speed vac. Peptides were dissolved in 1 ml of 10 mM ammonium hydroxide for subsequent high-pH fractionation.

High-pH fractionation. Peptides were loaded onto a C18 BEH XBridge column (130 Å, 3.5 µm, 4.6 mm × 250 mm, Waters), and a binary buffer system was used for peptide separation: buffer A, 10 mM ammonium hydroxide; buffer B, 10 mM ammonium hydroxide in 90% ACN. Within the 27-min gradient, the buffer B content was linearly increased over time to 38% over 19 min, followed by ramping to 80% and a re-equilibration step to 5% buffer B. Every 12th fraction was pooled and concentrated in a speed vac to complete dryness. Peptides were resuspended in 200 µl of 2.5% ACN and 2% formic acid. 3 µl was then used for liquid chromatography coupled with tandem mass spectrometry (LC–MS/MS) measurement.

Liquid chromatography and mass spectrometry. Instrumentation consisted of an EASY-nLC 1000 coupled to a Q Exactive Plus instrument. For peptide separation, we used a 50-cm in-house packed column (internal diameter (I.D.) 75 µm, C18 1.7 µm, Dr. Maisch beads) at a controlled temperature of 50 °C. The total gradient time was 60 min, and increasing acetonitrile content was used as described previously[44]. MS level1 spectra were acquired at 70,000 (200 m/z) resolution using 3×10^6 as an automated gain control (AGC) target. The instrument was operated in data-dependent mode, and the top ten most intense peaks were subsequently selected for fragmentation in the HCD collision cell applying a normalized collision energy of 27. The resolution was set to 17,500 and a maximal injection of 60 ms using an AGC target of 5×10^5 allowed maximal parallelization of filling and measuring of MS2 events. Dynamic exclusion was enabled for 30 s.

MaxQuant Analysis and Bioinformatics. All raw files were processed with MaxQuant 1.5.3.8 (ref. 45) and the implemented Andromeda search engine[46]. MS/MS spectra were correlated to the UniProt Mouse reference proteome (downloaded in 2016). Peptides were generated *in silico* using 2 miss cleavages, meaning that peptides might contain a maximal number of 3 lysines. Methionine oxidation and *n*-term acetylation were variable modifications, while carbamidomethylation at cysteine residues was defined as a fixed modification. Searches were performed using default settings for mass tolerances, and the requantify as well as the match-between algorithms were enabled. For SILAC-based quantification, a minimal ratio count of 1 was required.

The proteinGroups.txt file was filtered for contaminants and reverse hits. SILAC ratios were $\log_2$ transformed and normalized by subtraction of the median value, assuming that the majority of proteins do not change and to correct for unequal starting material. The $\log_2$ ratio was calculated by subtracting the mean of each group from the other experimental group. *P* values were obtained by performing unpaired two-tailed Student's *t*-tests. Gene Ontology annotations were retrieved from the UniProt database implemented in Perseus software[47]. 1D enrichment was then used to determine significantly changed groups of proteins[19]. Additionally, gene set enrichment analysis was performed through the Functional Annotation Tools from DAVID Bioinformatics Resources[20,48] using the selected genes that either had upregulated expression in the livers of LNA-miR-676-treated mice compared to the control LNA–treated mice (fold change ≥ 1.5, $P < 0.10$) or were detected exclusively in the livers of LNA-miR-676-treated mice.

Stimulation with recombinant EDA *in vitro* and *in vivo*. Stimulation experiments with recombinant EDA proteins were performed using recombinant active forms of mouse EDA-A1 (Ala179–Ser391, R&D Systems) and human EDA-A2 (Ala179–Ser389, R&D Systems). For the *in vitro* study, cells were stimulated with the recombinant proteins at a concentration of 500 ng/ml, whereas in the *in vivo* study wild-type mice at 8 weeks of age were administered 10 µg of the recombinant proteins intravenously at 10 a.m. without fasting. Samples were collected at the indicated time points and were directly frozen in liquid nitrogen.

AAV-mediated overexpression of *Eda-A2*. Serotype 8 AAV (AAV/8) was used. p87 vector harboring a mouse *Ttr* promoter was designed for production of AAV/8 inverted terminal repeat (ITR)-flanked self-complementary AAV vector genomes. The sequence encoding the extracellular domain of mouse EDA-A2 (amino acids Ala179–Ser389) preceded by an N-terminal signal sequence and two Flag epitope tag sequences was cloned into the p87 vector (p87-*Eda-A2*). For production of AAV/8 particles, the p87-*Eda-A2* plasmid or pscAAV-eGFP plasmid as a control was cotransfected with the AAV/8 helper plasmid pXR8 (kindly provided by J. Wilson, University of Pennsylvania) and the adenoviral helper plasmid pXX6-80 (kindly provided by J. Samulski, University of North Carolina) into HEK293 cells by calcium phosphate transfection. 48 h after transfection, cells were lysed and subjected to benzonase treatment. AAV particles were purified using a discontinuous iodixanol gradient (15–60%). The titers of the AAV viruses were determined by real-time qPCR. C57BL/6 mice were fed a HFD from 4 weeks of age and intravenously injected with the AAV viruses at a titer of 2×10^{10} particles/animal at 8 weeks of age. Indirect calorimetry was performed at 5 weeks after injection. The insulin tolerance test and the glucose tolerance test were performed at 6–7 weeks after injection. Tissues were collected for mRNA and protein analyses at 10 weeks after injection. Plasma Flag immunoblotting was conducted using plasma from an independent pilot cohort of AAV-injected C57BL/6 mice under NCD feeding at indicated time points after injection.

AAV-mediated suppression of *Eda* expression. Serotype DJ8 AAV (AAV/DJ8) encoding an shRNA sequence targeting mouse *Eda* or control scrambled shRNA under the control of the U6 promoter was produced by Vector Biolabs. The targeted sequence was 5′-CCAACTACAACACTTGCTATACT-3, located in the last exon, which is common to all isoforms encoded by *Eda*. Mice were intravenously injected with AAV viruses at a titer of 2×10^{10} to 3×10^{10} particles/animal. The insulin tolerance test and glucose tolerance test were performed at 2 and 3 weeks after AAV injection, respectively. The hyperinsulinemic–euglycemic clamp study was performed at 3 weeks after AAV injection using a separate cohort of mice. After metabolic assays, the mice were euthanized and subjected to analysis, including gene expression measurements.

Indirect calorimetry and food intake measurement. All measurements were performed in a PhenoMaster System (TSE systems), which allowed metabolic performance measurement and activity monitoring by an infrared light-beam frame. Mice were placed at room temperature (22 °C–24 °C) in 7.1-l chambers of the PhenoMaster open-circuit calorimetry. Mice were allowed to acclimatize in the chambers for at least 24 h. Food and water were provided *ad libitum* in the appropriate devices and measured by the built-in automated instruments. The parameters of indirect calorimetry were measured for at least 48 h. Presented data are average values obtained in these recordings.

Metabolic assays. For insulin tolerance tests, mice were injected with 0.8 IU per kg body weight of insulin (Insuman rapid, Sanofi-Aventis) intraperitoneally at 9 a.m. without fasting. For glucose tolerance tests, mice were injected with 2 g per kg body weight of glucose intraperitoneally after fasting for 6 h, except for *db*/*db* mice, which were injected with 1 g per kg body weight of glucose intraperitoneally after fasting for 16 h. Blood samples were collected at the indicated time points, and blood glucose levels were determined by Contour (Bayer).

Hyperinsulinemic–euglycemic clamp study. Surgical implantation of catheters in the jugular vein was performed as previously described[49]. After 4–7 d of recovery, animals were fasted for 16 h. All infusions used in the experiment were prepared using a 3% plasma solution obtained from donor animals. Infusion with a continuous tracer, D-[3-^{3}H]glucose, was started 50 min before

doi:10.1038/nm.4420

the clamp (PerkinElmer, 0.05 µCi/min after priming with 5 µCi). After a 50-min basal period, a blood sample (60 µl) was collected from the tail tip for determination of basal parameters. The clamp started with a continuous insulin infusion (Insuman rapid, Sanofi-Aventis; 20 µU/g/min after priming with 120 µU/g, and blood glucose levels were measured every 10 min using Contour (Bayer). The infusion rate of 20% was adjusted to maintain glucose at the target level (140 mg/dl). 120 min before the end of the experiment, 2-[1-^{14}C]deoxy-D-glucose (2DG) (American Radiolabeled Chemicals, 10 µCi) was infused, and blood samples (15 µl) were collected until steady state was reached. Steady state was ascertained when a fixed GIR maintained blood glucose measurements at a constant level for 30 min. During the steady state, blood samples (60 µl) were collected for the measurement of steady-state parameters. At the end of the experiment, mice were killed by cervical dislocation, and tissues were collected at −80 °C. Plasma [3-^{3}H]glucose radioactivity at basal and steady-state levels was measured as previously described[50]. Plasma 2DG radioactivity was directly measured in a liquid scintillation counter. Tissue lysates were processed through ion-exchange chromatography columns (Poly-Prep Prefilled Chromatography Columns, AGR1-X8 formate resin, 200–400 mesh dry; Bio-Rad) to separate 2DG from 2-[1-^{14}C]deoxy-D-glucose-6-phosphate (2DG6P). The glucose turnover rate ($mg \times kg^{-1} \times min^{-1}$) was calculated as previously described[50]. *In vivo* glucose uptake for adipose tissues and skeletal muscles ($mmol \times g^{-1} \times min^{-1}$) was calculated based on the accumulation of 2DG6P in measured tissue, and the disappearance rate of 2DG from plasma was calculated as described previously[51].

RNA-seq analyses. Eight libraries were prepared using the Illumina TruSeq RNA Sample Preparation Kit. Library preparation started with 1 µg of total RNA. After poly(A) selection (using poly(T)-oligonucleotide-attached magnetic beads), mRNA was purified and fragmented using divalent cations under an elevated temperature. RNA fragments underwent reverse transcription using random primers. This was followed by second-strand cDNA synthesis with DNA polymerase I and ribonuclease H. After end repair and A-tailing, indexing adaptors were ligated. The products were then purified and amplified (14 PCR cycles) using 10 µl of template to create the final cDNA libraries. After library validation and quantification (Agilent Tape Station), equimolar amounts of library were pooled. Pools were quantified using the Peqlab Kapa Library Quantification Kit and the Applied Biosystems 7900HT Sequence Detection System. Pools were then sequenced using two lanes of an Illumina HiSeq 4000 sequencer run with a paired-end ($76 \times 7 \times 76$ cycles) protocol. RNA-seq data were analyzed using the QuickNGS analysis system[52], version 1.2.1, on release 82 of the Ensembl database. The list of analysis algorithms adopted by this pipeline can be reviewed at http://bifacility.uni-koeln.de/quickngs/web/doc/algorithms.php/. For statistical analyses, P values were obtained by performing unpaired two-tailed Student's t-tests, and for selected genes (fold change ≥ 1.2, $P < 0.05$) gene set enrichment analysis was performed using the Functional Annotation Tool from the DAVID Bioinformatics Resources[20,48].

Statistical analyses. All analyses were performed with GraphPad Prism version 6.0b. Unless otherwise specified, data sets were analyzed for statistical significance using an unpaired two-tailed Student's t-test or one-way ANOVA with the Holm–Sidak multiple-comparisons test. The normality of distributions was calculated with the D'Agostino and Pearson omnibus normality test where applicable. For calculations of the equality of variance in one-way ANOVA, the Brown–Forsythe test was used. Statistical analyses for correlation in human data were performed using Spearman's correlation.

Data availability. The small RNA-seq data have been deposited in NCBI and are available under BioProject accession number PRJNA392220. The RNA-seq data for muscle from *db*/*db* mice with *Eda* suppression have been deposited in the Gene Expression Omnibus and are available under accession number GSE100686. The mass spectrometry proteomics data for liver from *db*/*db* mice with miR-676 suppression have been deposited at the ProteomeXchange Consortium via the proteomics identifications (PRIDE)[53] partner repository with data set identifier PXD006573. A **Life Sciences Reporting Summary** is available.

40. Awazawa, M. *et al.* Adiponectin suppresses hepatic SREBP1c expression in an AdipoR1/LKB1/AMPK dependent pathway. *Biochem. Biophys. Res. Commun.* **382**, 51–56 (2009).
41. Amrutkar, M. *et al.* Protein kinase STK25 controls lipid partitioning in hepatocytes and correlates with liver fat content in humans. *Diabetologia* **59**, 341–353 (2016).
42. Kannt, A. *et al.* Association of nicotinamide-*N*-methyltransferase mRNA expression in human adipose tissue and the plasma concentration of its product, 1-methylnicotinamide, with insulin resistance. *Diabetologia* **58**, 799–808 (2015).
43. Krüger, M. *et al.* SILAC mouse for quantitative proteomics uncovers kindlin-3 as an essential factor for red blood cell function. *Cell* **134**, 353–364 (2008).
44. Wai, T. *et al.* The membrane scaffold SLP2 anchors a proteolytic hub in mitochondria containing PARL and the i-AAA protease YME1L. *EMBO Rep.* **17**, 1844–1856 (2016).
45. Cox, J. & Mann, M. MaxQuant enables high peptide identification rates, individualized p.p.b.-range mass accuracies and proteome-wide protein quantification. *Nat. Biotechnol.* **26**, 1367–1372 (2008).
46. Cox, J. *et al.* Andromeda: a peptide search engine integrated into the MaxQuant environment. *J. Proteome Res.* **10**, 1794–1805 (2011).
47. Tyanova, S. *et al.* The Perseus computational platform for comprehensive analysis of (prote)omics data. *Nat. Methods* **13**, 731–740 (2016).
48. Huang, W., Sherman, B.T. & Lempicki, R.A. Bioinformatics enrichment tools: paths toward the comprehensive functional analysis of large gene lists. *Nucleic Acids Res.* **37**, 1–13 (2009).
49. Könner, A.C. *et al.* Insulin action in AgRP-expressing neurons is required for suppression of hepatic glucose production. *Cell Metab.* **5**, 438–449 (2007).
50. Fisher, S.J. & Kahn, C.R. Insulin signaling is required for insulin's direct and indirect action on hepatic glucose production. *J. Clin. Invest.* **111**, 463–468 (2003).
51. Ferré, P., Leturque, A., Burnol, A.F., Penicaud, L. & Girard, J. A method to quantify glucose utilization *in vivo* in skeletal muscle and white adipose tissue of the anaesthetized rat. *Biochem. J.* **228**, 103–110 (1985).
52. Wagle, P., Nikolić, M. & Frommolt, P. QuickNGS elevates next-generation sequencing data analysis to a new level of automation. *BMC Genomics* **16**, 487 (2015).
53. Vizcaíno, J.A. *et al.* 2016 update of the PRIDE database and its related tools. *Nucleic Acids Res.* **44**, 11033 (2016).

Corresponding Author: Jens C. Brüning

Date: 09/09/2017

Life Sciences Reporting Summary

Nature Research wishes to improve the reproducibility of the work we publish. This form is published with all life science papers and is intended to promote consistency and transparency in reporting. All life sciences submissions use this form; while some list items might not apply to an individual manuscript, all fields must be completed for clarity.

For further information on the points included in this form, see Reporting Life Sciences Research. For further information on Nature Research policies, including our data availability policy, see Authors & Referees and the Editorial Policy Checklist.

Experimental design

1. Sample size

   Describe how sample size was determined.

   Sample sizes for animal experiments were calculated based on power calculations with an alpha of 0.8 and were chosen based on experience from previous in house studies of metabolic phenotyping and to balance between the ability to detect significance differences while reducing the number of animals used.

2. Data exclusions

   Describe any data exclusions.

   No data were excluded from the studies.

3. Replication

   Describe whether the experimental findings were reliably reproduced.

   Cell culture experiment results (Fig. 1h, 3b, 3d, 3f-h, Supplementary fig. 7 lower panel) were reproduced at least three times. All other attempts for replication were successful.

4. Randomization

   Describe how samples/organisms/participants were allocated into experimental groups.

   The samples and animals were randomely assigned to the experimental conditions.

5. Blinding

   Describe whether the investigators were blinded to group allocation during data collection and/or analysis.

   The experiments were conducted in a non-blinded way.

   Note: all studies involving animals and/or human research participants must disclose whether blinding and randomization were used.

6. Statistical parameters

   For all figures and tables that use statistical methods, confirm that the following items are present in relevant figure legends (or the Methods section if additional space is needed).

n/a	Confirmed	
☐	☒	The exact sample size (*n*) for each experimental group/condition, given as a discrete number and unit of measurement (animals, litters, cultures, etc.)
☐	☒	A description of how samples were collected, noting whether measurements were taken from distinct samples or whether the same sample was measured repeatedly.
☐	☒	A statement indicating how many times each experiment was replicated
☐	☒	The statistical test(s) used and whether they are one- or two-sided (note: only common tests should be described solely by name; more complex techniques should be described in the Methods section)
☐	☒	A description of any assumptions or corrections, such as an adjustment for multiple comparisons
☐	☒	The test results (e.g. *p* values) given as exact values whenever possible and with confidence intervals noted
☐	☒	A summary of the descriptive statistics, including central tendency (e.g. median, mean) and variation (e.g. standard deviation, interquartile range)
☐	☒	Clearly defined error bars

See the web collection on statistics for biologists for further resources and guidance.

Nature Medicine: doi:10.1038/nm.4420

Software

Policy information about availability of computer code

7. Software

Describe the software used to analyze the data in this study.	GraphPad PRISM ver 6.0b

For all studies, we encourage code deposition in a community repository (e.g. GitHub). Authors must make computer code available to editors and reviewers upon request. The *Nature Methods* guidance for providing algorithms and software for publication may be useful for any submission.

Materials and reagents

Policy information about availability of materials

8. Materials availability

Indicate whether there are restrictions on availability of unique materials or if these materials are only available for distribution by a for-profit company.	All the materials are available upon request.

9. Antibodies

Describe the antibodies used and how they were validated for use in the system under study (i.e. assay and species).	Antibodies against phospho-SAPK/JNK (Thr183/Thr185) (#4668), SAPK/JNK (#9252) and DYKDDDDK Tag (#2368, Binds to same epitope as Sigma's Anti-FLAG® M2 Antibody) were purchased from Cell Signaling Technology and used at 1:2000 dilution. For IRS1 immunoblot, Anti-IRS1 antibody purchased from BD Biosciences (611395) was used at 1:1000 dilution, except for Fig. 4i, where anti-IRS1 antibody purchased from Abcam (ab131487) was used at 1:1000 dilution. Anti-Calnexin antibody (#208880) was purchased from Calbiochem and used at 1:5000 dilution. Anti-phospho-IRS1 (Ser307) (ab5599) was purchased from Abcam and used at 1:2000 dilution. Anti-EDA-A1 mouse monoclonal antibody Renzo-2 was available from Enzo Life Sciences (ALX-522-038) and used at 1:1000 dilution. The secondary antibody Anti-Rabbit IgG-Peroxidase antibody (A6154) or Anti-Mouse IgG-Peroxidase antibody (A4416) was purchased from Sigma-Aldrich and used at 1:5000 dilution, except for the blot using anti-IRS1 antibody (BD Bioscience) where the secondary antibody was used at 1:1000 dilution.

10. Eukaryotic cell lines

a. State the source of each eukaryotic cell line used.	The cells were obtained from American Type Culture Collection (ATCC).
b. Describe the method of cell line authentication used.	Not applicable.
c. Report whether the cell lines were tested for mycoplasma contamination.	The cells were tested negative for mycoplasma contamination
d. If any of the cell lines used in the paper are listed in the database of commonly misidentified cell lines maintained by ICLAC, provide a scientific rationale for their use.	Not applicable.

Animals and human research participants

Policy information about studies involving animals; when reporting animal research, follow the ARRIVE guidelines

11. Description of research animals

Provide details on animals and/or animal-derived materials used in the study.	BKS.Cg-Dock7m +/+ Leprdb/J (db/db) male mice or their control misty/misty male mice were purchased from Jackson Laboratory or Janvier Labs. C57BL/6JRj wild-type male mice were purchased from Janvier Labs. Eda-deficient Tabby mice were kindly provided by Pascal Schneider, Lausanne University. The mice carrying a constitutively-active version of JNK specifically in skeletal muscle were described previously (ref 41).

Nature Medicine: doi:10.1038/nm.4420

Policy information about studies involving human research participants

12. Description of human research participants

Describe the covariate-relevant population characteristics of the human research participants.

In a first cohort EDA mRNA expression was measured in liver tissue samples obtained from 33 men who underwent open abdominal surgery for Roux-en-Y bypass, sleeve gastrectomy, explorative laparotomy or elective cholecystectomy (Supplementary Table 4a). A small liver biopsy was taken during the surgery, immediately snap-frozen in liquid nitrogen, and stored at −80 °C until further preparations. All baseline blood samples and liver biopsies were collected between 8:00 hours and 10:00 hours after an overnight fast as described previously45.
In addition, we included 23 Caucasian obese patients (14 women, 9 men) who underwent a two-step bariatric surgery strategy with gastric sleeve resection as the first step and a Roux-en-Y- gastric bypass as second step 12 ± 2 months later (Supplementary Table 4b). At both time points, liver biopsies were obtained. General inclusion and exclusion criteria as well as methods for the measurement of anthropometric and laboratory parameters have been reported recently46. Study protocols have been approved by the ethics committee of the University of Leipzig (Reg. No. 031-2006 and 017-12-23012012). All participants gave written informed consent before taking part in the study.

Nature Medicine: doi:10.1038/nm.4420